Available online at www.sciencedirect.com
ScienceDirect
C. R. Chimie 11 (2008) 734–740
COMPTES RENDUS CHIMIE
http://france.elsevier.com/direct/CRAS2C/

Full paper / Mémoire

# Electron microscopy and structural studies of $Nd_{1/3}NbO_3$

Sabine Roudeau [a], François Weill [a,b], Stanislas Pechev [a], Jean-Marc Bassat [a], Jean-Claude Grenier [a,*]

[a] *ICMCB, CNRS, Université Bordeaux-1, 87, avenue du Docteur-Albert-Schweitzer, 33608 Pessac cedex, France*
[b] *Centre de ressource en microscopie électronique et microanalyse, CREMEM, Université Bordeaux-1, 350, cours de la Libération, 33400 Talence cedex, France*

Received 22 July 2007; accepted after revision 4 October 2007

**Abstract**

The crystal structure of the deficient perovskite $Nd_{1/3}NbO_3$ has been determined at room temperature, using electron microscopy observations and X-ray powder diffraction data. Electron diffraction study and HRTEM images evidence the doubling of *a* and *b* parameters and confirm one of the *c*-parameter with respect to perovskite unit cell. The structure refinement has been carried out using the orthorhombic *Cmmm* space group. The $Nd^{3+}$ cations occupy randomly and alternatively the (00l) planes and $Nb^{5+}$ cations distorted octahedral sites. This structure is characterized by the presence of empty $Nd^{3+}$ sites in every second layer and the tilting of the octahedral sites around the *b*-axis. In addition, electron diffraction patterns exhibit weak additional diffuse reflections, which supposes some ordering of the Nd vacancies. ***To cite this article: S. Roudeau et al., C. R. Chimie 11 (2008).***


**Résumé**

La structure cristalline de la perovskite $Nd_{1/3}NbO_3$ lacunaire en néodyme a été déterminée à température ambiante sur la base de données de microscopie électronique et de diffraction X. Les clichés de diffraction électronique ainsi que les images de haute résolution montrent un doublement des paramètres *a* et *b* et confirment celui du paramètre *c*. L'affinement de la structure a été réalisé avec le groupe spatial *Cmmm*. Les cations $Nd^{3+}$ occupent statistiquement et alternativement les plans (00l) et les cations $Nb^{5+}$ des sites octaédriques distordus. La structure est caractérisée par la présence de sites vides de $Nd^{3+}$ dans un plan sur deux selon l'axe *c* et par une inclinaison des octaèdres autour de l'axe *b*. De faibles réflexions diffuses sont visibles dans les clichés de diffraction électronique, qui pourraient être dues à un ordre local des lacunes de néodyme. ***Pour citer cet article : S. Roudeau et al., C. R. Chimie 11 (2008).***


*Keywords:* Perovskite, Niobate; Crystal structure; Electron microscopy; Cation ordering

*Mots-clés :* Perovskite, Niobiate ; Structure cristalline ; Microscopie électronique, Ordre cationique

* Corresponding author.
*E-mail address:* grenier@icmcb-bordeaux.cnrs.fr (J.-C. Grenier).

1631-0748/$ - see front matter © 2007 Académie des sciences. Published by Elsevier Masson SAS. All rights reserved.
doi:10.1016/j.crci.2007.10.002

## 1. Introduction

The ideal perovskite has the general formula $ABX_3$, where the A-site cations are typically larger than the B-site ones and similar in size to the X-site anions. In this structure, the A cations are surrounded by 12 anions in cubo-octahedral coordination and the B cations are surrounded by 6 anions in octahedral coordination. The ideal structure adopts the cubic space group $Pm\bar{3}m$ [1].

One of the most important characteristics of perovskite-related structures is their compositional flexibility. This structure can tolerate anionic non-stoichiometry in the X-site as well as cationic deficiency in the A-site. Cation-deficient perovskite-type oxides $A_{1-x}BO_3$ have been studied for a number of years. Compounds with B = W, Mo or Re are named "bronzes" and A (usually alkali metal) occupies a random position; those with Ti, Nb or Ta, namely "non-stoichiometric perovskites", exhibit some ordering of A cations. Their structure consists of the framework of $BO_6$ octahedra with partially occupied layers of A-site cations alternating with A-vacant layers along the *c*-axis resulting in a doubling of the perovskite cell along the *c*-axis (Fig. 1). Several $A_{1-x}BO_3$ perovskite oxides do exist, such as $Ln_{2/3}TiO_3$ [2,3], $Ln_{1/3}BO_3$ (B = Nb, Ta) [4–9] or $Th_{1/4}NbO_3$ [10]. For this latter compound, an additional long-range ordering between Th atoms and vacancies, giving rise to modulation or localized diffusion, has been detected by electron and X-ray diffraction. This kind of material has also been shown to exhibit interesting properties as electrodes for the Li ion insertion reactions in batteries or for their dielectric behavior and magnetic response [11–14].

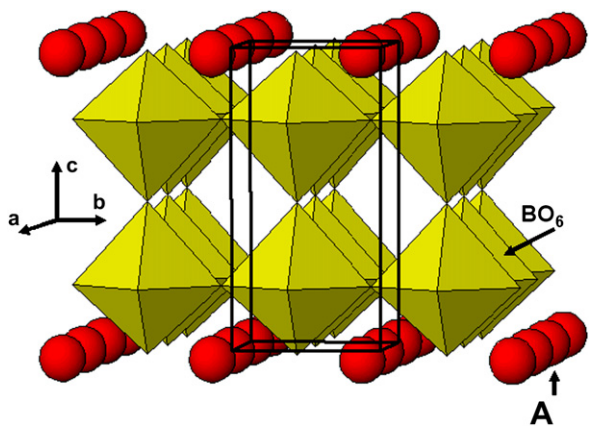


Fig. 1. Idealized structure of $A_{1-x}BO_3$: B = Ti ($x = 0.33$) or Nb ($x = 0.66$) showing the half (00l) empty planes and half (001) partially filled planes.

The crystal structure of $Nd_{1/3}NbO_3$ was first reported by Iyer et al. [9] as isotype of β-$La_{1/3}NbO_3$, in which the lanthanide ions order into alternate (00l) planes, doubling the *c*-parameter. $Nd_{1/3}NbO_3$ crystallizes in the orthorhombic space group *Pmmm* with cell parameters $a = 3.878$ Å, $b = 3.907$ Å and $c = 7.840$ Å (Table 1) at room temperature. Later on, Carrillo et al. [15], using electron microscopy, observed a superstructure in β-$La_{1/3}NbO_3$ ($2a \times 2b \times c$). Nevertheless, their X-ray diffraction data, even with a careful analysis, did not reveal any features which could be related to the presence of the superstructure observed by electron microscopy. Thus, they interpreted the superstructure as resulting from distorted octahedra on the basis of simulation of the X-ray diffraction patterns.

The aim of the present work is to characterize $Nd_{1/3}NbO_3$ using XRD (Rietveld refinement) and electron microscopy observations in order to establish whether the superstructure observed in β-$La_{1/3}NbO_3$ is present or not in this compound.

## 2. Experimental

Powder of $Nd_{1/3}NbO_3$ was obtained by solid-state reaction. The starting materials $Nd_2O_3$ and $Nb_2O_5$ oxides (Aldrich, purity 99.9%) were first dried in air, at 1000 °C, for 24 h. A stoichiometric mixture of these oxides was ground with ethanol in an agate mortar and then heated in an alumina crucible at 1100 °C in air for 10 h, and, after intermediate regrinding, at 1300 °C for 36 h, in air.

The XRD pattern of $Nd_{1/3}NbO_3$ was recorded at room temperature on a Philip X'pert Pro powder diffractometer in the Bragg–Brentano geometry with a back monochromator, using Cu $K\alpha_1$ radiations ($\lambda = 1.5406$ Å). The data collection was performed in the 6–130° $2\theta$ range with a 0.0080° step, using an X'celerator detector (linear PSD covering 2.122 mm).

The diffraction data were analyzed using the Rietveld technique as implemented in the Fullprof program

Table 1
Structural data of $Nd_{1/3}NbO_3$ from Iyer et al. [9]

| $Nd_{1/3}NbO_3$ | |
|---|---|
| Crystal system | Orthorhombic |
| Space group | *Pmmm* |
| *Z* | 8 |
| Lattice parameters (Å) | $a = 3.8807$ (1) $b = 3.9067$ (1) $c = 7.8365$ (1) $\alpha = \beta = \gamma = 90$ °C |
| Volume (Å$^3$) | 118.8 |

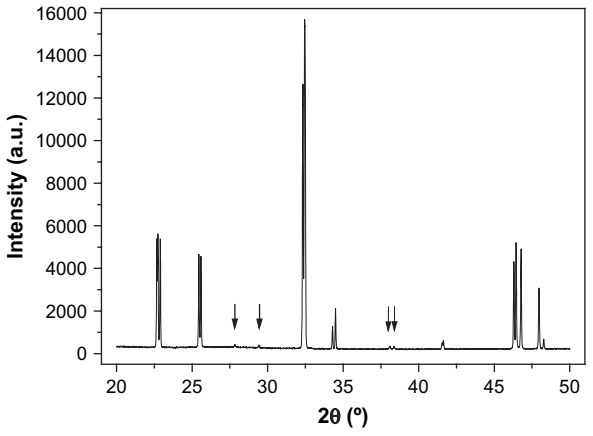


Fig. 2. XRD pattern of $Nd_{1/3}NbO_3$ at room temperature; the arrows indicate the reflection not indexed in the $a = 3.881$ Å, $b = 3.907$ Å, $c = 7.836$ Å cell.

(software winPLOTR, version June 2005 LLB Saclay – LCSIM Rennes).

Electron diffraction experiments were carried out with a JEOL 2000FX electron microscope equipped with a double-tilt specimen stage. The powder was crushed in ethanol and a drop of this suspension was then deposited on a holey carbon-supported film. High-resolution images were obtained using a JEOL 2200FS microscope.

## 3. Results and discussion

### 3.1. X-ray powder diffraction

The X-ray diffraction pattern of the as-prepared material, $Nd_{1/3}NbO_3$, is shown in Fig. 2. Most of the reflections can be indexed in the orthorhombic system with the following cell parameters, $a = 3.881$ Å, $b = 3.907$ Å, $c = 7.836$ Å, close to the ones previously reported in the literature for this compound [9]; however, additional reflections can be noted (arrows in the figure). Further heat treatments at 1300 °C did not modify the X-ray diffraction pattern. Annealing at higher temperatures up to fusion ($\approx$1400 °C) led to a decomposition into $NdNbO_4$ and $Nb_2O_5$. In order to understand the origin of these additional reflections, electron diffraction was then performed.

### 3.2. Electron diffraction

Typical electron diffraction patterns of $Nd_{1/3}NbO_3$ powder are shown in Fig. 3. Using the $c^*$ axis which

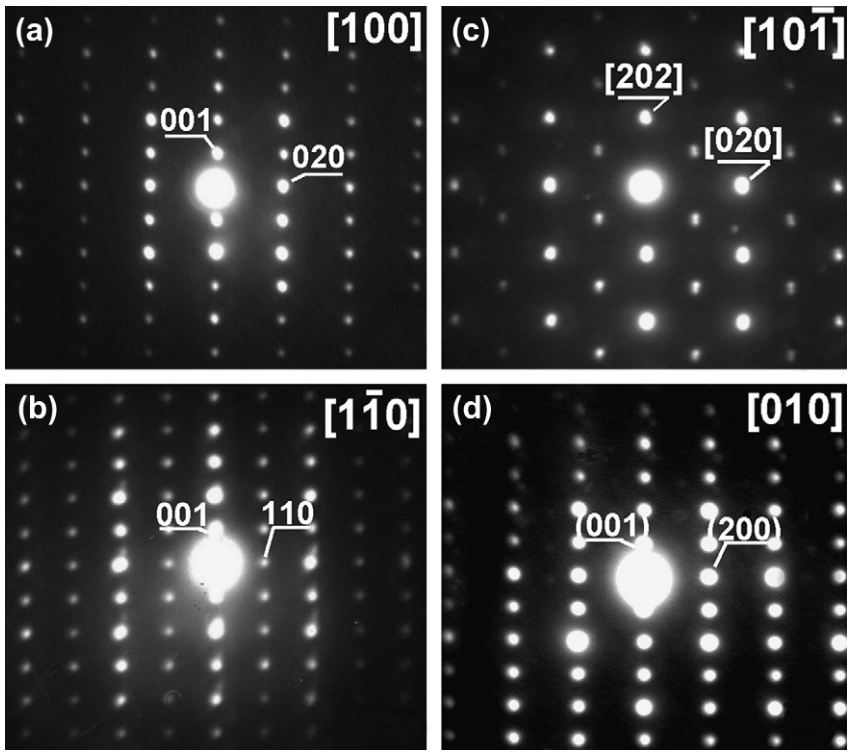


Fig. 3. Electron diffraction patterns for $Nd_{1/3}NbO_3$: zone axes (a) [100], (b) [1$\bar{1}$0], (c) [10$\bar{1}$] and (d) [010].

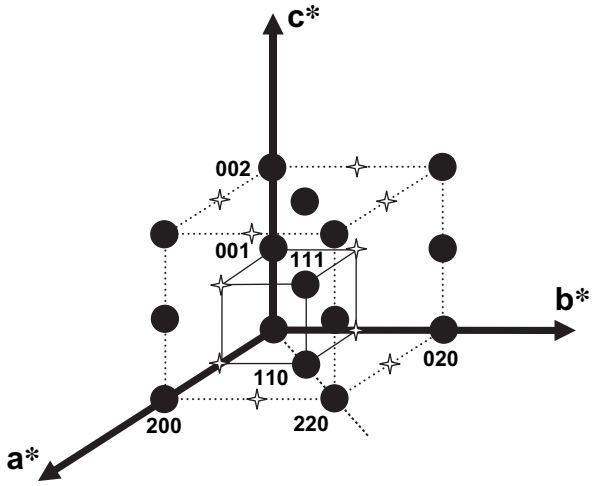


Fig. 4. Reciprocal lattice for $Nd_{1/3}NbO_3$ characterizing the C-type Bravais lattice.

can be easily identified ($\approx$7.8 Å), Fig. 3a characterizes the [100] zone axis; tilting of about 45° around the $c^*$ axis leads to pattern (3*b*). To be fully interpreted, this pattern needs to double the *a* and *b* initial parameters. Obviously for instance, the reflection labeled (110) cannot be indexed without doubling *a* and *b* parameters. Thus, this pattern corresponds to $[1\bar{1}0]$ zone axis. Starting from the pattern (3*a*) ([100] zone axis) and tilting of about 45° around the $b^*$ axis leads to pattern (3*c*) corresponding to the $[10\bar{1}]$ zone axis. This pattern further confirms the superstructure $2a \times 2b$. Starting from the $[1\bar{1}0]$ zone axis, any rotation of 45° around the $c^*$ axis gives patterns similar to Fig. 3d or a. Note that the $a^*$ and $b^*$ axes cannot be distinguished as they are metrically almost identical. The reciprocal lattice (Fig. 4) reconstructed from these patterns implies as for the X-ray data, a superstructure with the following cell parameters: $a_C \approx 7.76$ Å, $b_C \approx 7.81$ Å, $c_C \approx 7.84$ Å. From the systematic condition of reflections $h + k = 2n$, which appears in the patterns, a C Bravais lattice can be deduced. Since we did not observe any additional conditions in the $(0kl)^*$ and $(h0l)^*$ reciprocal planes, the absence of glide planes orthogonal to *a* and *b* directions can be asserted.

Unfortunately it has not been possible to get information on a possible presence of a glide plane orthogonal to the *c* direction, as the $(hk0)^*$ reciprocal plane has not been observed.

In addition, one should stress that in most patterns, after long exposure, additional spots of weak or very weak intensity, more or less diffuse, can be evidenced, as shown in Fig. 5. The previous cell describes the main reflections but not the very weak additional ones which are observed around the main spots. These additional reflections are reproducible and present in various reciprocal planes. Due to their very weak intensity, it has not been possible to obtain additional information such as the exact location of these diffuse scattering or even their nature (spots, surface, cylinder, sphere…).

### 3.3. Rietveld structural refinements

On the basis of the electron diffraction study, the X-ray diffraction pattern of $Nd_{1/3}NbO_3$ was then refined using the Fullprof program. With respect to the work of Carillo et al. [15], the most symmetrical space group, i.e. *Cmmm*, was chosen with the initial cell parameters obtained from the previous electron diffraction study. In a first refinement, the initial atomic positions of $Nd_{1/3}NbO_3$ were deduced from those of $La_{1/3}NbO_3$ [15]. In the course of this work, Zhang et al. published the crystal structure of $Nd_{1/3}NbO_3$ based on neutron diffraction data [16]. A second refinement was therefore performed using the atomic positions (*Cmmm* space

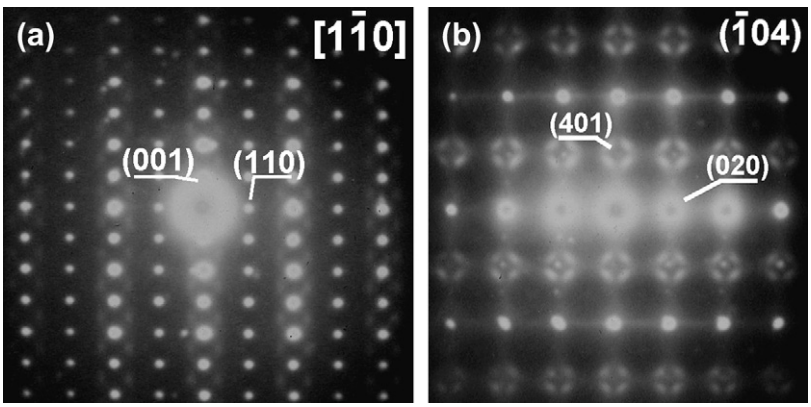


Fig. 5. Electron diffraction patterns of the $[1\bar{1}0]$ (a) and $[\bar{1}04]$ (b) zone axes for $Nd_{1/3}NbO_3$ showing weak additional spots.

Table 2
Structural data and X-ray Rietveld refinement parameters at room temperature of $Nd_{1/3}NbO_3$

| $Nd_{1/3}NbO_3$ | Positions from Carillo [15] | Positions from Zhang [16] |
|---|---|---|
| Crystal system | Orthorhombic | Orthorhombic |
| Space group | *Cmmm* | *Cmmm* |
| *Z* | 8 | 8 |
| *a* (Å) | 7.7614 (1) | 7.7614 (1) |
| *b* (Å) | 7.8134 (1) | 7.8134 (1) |
| *c* (Å) | 7.8364 (1) | 7.8365 (1) |
| Volume (Å$^3$) | 475.22 | 475.23 |
| Theoretical density (g cm$^{-3}$) | 5.28 | 5.28 |
| Experimental density (g cm$^{-3}$) | 5.27 | 5.27 |
| Wavelength (Å) | $\lambda K_{\alpha 1} = 0.15406$ | $\lambda K_{\alpha 1} = 0.15406$ |
| Step scan increment (deg 2$\theta$) | 0.008 | 0.008 |
| 2$\theta$ range (deg) | 7–130 | 7–130 |
| Program | Fullprof | Fullprof |
| Scale factor | $0.1882 \times 10^{-3}$ | $0.2221 \times 10^{-3}$ |
| Zero point (deg 2$\theta$) | −0.0083 | −0.0078 |
| Pseudo-Voigt function [PV = $\eta L + (1-\eta))G$] | $\eta = 0.2729$ (4) | $\eta = 0.2801$ (4) |
| Caglioti law parameters | $U = 0.01137$ | $U = 0.01109$ |
| | $V = -0.00184$ | $V = -0.00160$ |
| | $W = 0.00290$ | $W = 0.00285$ |
| No. of reflections | 264 | 264 |
| No. of refined parameters | 31 | 30 |
| $R_{Bragg}$ | 6.35 | 4.72 |
| $cR_{wp}$ (%) | 14.2 | 13.2 |
| $cR_{exp}$ (%) | 11.69 | 11.69 |
| $\chi^2$ | 1.47 | 1.28 |

group). We also included a second phase, $NdNbO_4$, which could be identified in small amount. This resulted in a slightly improved refinement.

The peak shape was described by a pseudo-Voigt function, and the background level was fitted with linear interpolation between a set of 28 given points with refinable heights. The refined parameters include the scale factor, zero point correction, cell parameters, isotropic thermal and positional parameters for all atoms and three coefficients to describe the angular dependence of line width and asymmetry factors.

Data and details of the refinements are given in Table 2. The various reliability factors show that the refinement # 2, based on the atomic positions of Zhang et al., is improved, the final values being $R_{exp} = 11.69$; $R_{wp} = 13.2$; $R_B = 4.72$; $\chi^2 = 1.28$.

Fig. 6 shows the excellent agreement between the calculated and observed diffraction profiles for $Nd_{1/3}NbO_3$. The atomic positions, isotropic thermal displacement and reliability factors ($R_B$ and $R_{wp}$) of $Nd_{1/3}NbO_3$ are given in Table 3 and the interatomic distances in Table 4, only for the refinement based on Zhang atomic positions.

Additional efforts for positioning some amount of Nd in the empty plane and fitting with other space groups of lower symmetry were carried out without success. In all cases, the goodness of the fit did not improve. Finally, the amount of the impurity, $NdNbO_4$, was estimated to be around 1–2%.

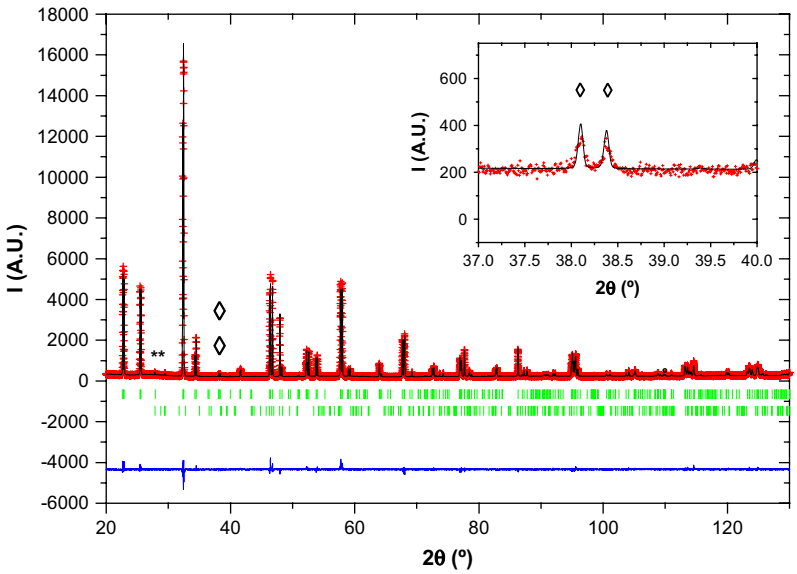


Fig. 6. Rietveld refinement of the powder XRD pattern of $Nd_{1/3}NbO_3$. The observed (+), calculated (—), and difference (bottom line) profiles, as well as Bragg positions (vertical bars) are shown. (*) Indicates peak positions of secondary phase $NdNbO_4$ (JPDS 85–1110). (◇) Indicates positions of characteristic superstructure peaks.

Table 3
Atomic positions, isotropic thermal displacement and reliability factors of $Nd_{1/3}NbO_3$

| Atom | Site | $x$ | $y$ | $z$ | $B$ | Occ. |
|---|---|---|---|---|---|---|
| # 1 – $Nd_{1/3}NbO_3$ (from Carillo) | | | | | | |
| $a = 7.7614$ Å, $b = 7.8134$ Å, $c = 7.8364$ Å, $R_B = 6.35$, $R_{wp} = 14.2$ | | | | | | |
| Nd (1) | 2a | 0 | 0 | 0 | 0.41 (52) | 0.080 |
| Nd (2) | 2b | 0.5 | 0 | 0 | 0.34 (46) | 0.088 |
| Nb | 8m | 0.25 | 0.25 | 0.260 (1) | 0.46 (4) | 0.5 |
| O (1) | 8n | 0 | 0.248 (9) | 0.230 (2) | 1.88 (32) | 0.5 |
| O (2) | 8o | 0.228 (4) | 0 | 0.226 (2) | 0.73 (40) | 0.5 |
| O (3) | 4e | 0.25 | 0.25 | 0 | 3.31 (60) | 0.25 |
| O (4) | 4f | 0.25 | 0.25 | 0.5 | 2.95 (57) | 0.25 |
| # 2 – $Nd_{1/3}NbO_3$ (from Zhang) | | | | | | |
| $a = 7.7614$ Å, $b = 7.8134$ Å, $c = 7.8365$ Å, $R_B = 4.72$, $R_{wp} = 13.2$ | | | | | | |
| Nd | 4i | 0 | 0.251 (1) | 0 | 0.56 (4) | 0.1667 |
| Nb | 8o | 0.250 (2) | 0 | 0.261 (1) | 0.70 (3) | 0.5 |
| O (1) | 4g | 0.285 (1) | 0 | 0 | 1.82 (47) | 0.25 |
| O (2) | 4h | 0.218 (1) | 0 | 0.5 | 1.95 (47) | 0.25 |
| O (3) | 4k | 0 | 0 | 0.196 (1) | 0.67 (42) | 0.25 |
| O (4) | 4l | 0 | 0.5 | 0.271 (1) | 0.29 (40) | 0.25 |
| O (5) | 8m | 0.25 | 0.25 | 0.229 (1) | 1.42 (22) | 0.5 |

### 3.4. Discussion: structural features

The structure of $Nd_{1/3}NbO_3$ is known to be of the deficient A-site perovskite type, with $Nb^{5+}$ and $Nd^{3+}$ ions located in octahedral and in dodecahedral sites, respectively. The refinement of the XRD pattern confirms the presence of empty $Nd^{3+}$ sites in every second layer. The high-resolution image (Fig. 7) is consistent with this structure and evidences the cation ordering; the inset shows a simulated image calculated with the structural data obtained from the X-ray refinement that nicely confirms these results. This makes a framework of $NbO_6$ octahedra and partially occupied layers of $Nd^{3+}$ cations at $z = 0$, alternating with Nd-vacant layers ($z = 1/2$), which causes the $c$-axis to be doubled (Fig. 8). At $z = 0$, $Nd^{3+}$ ions occupy partially and randomly the dodecahedral sites in agreement with both refinements, the average composition being $Nd_{1/3}NbO_3$. In addition, $Nb^{5+}$ atoms are slightly shifted from the octahedra center towards the empty Nd layer, which results in alternating long and short Nb–O bonds along the $c$-axis (*cf.* Nb–$O_1$ and Nb–$O_2$ in Table 4). Similarly, $O_3$, $O_4$ and $O_5$ atoms are slightly moved away from their ideal positions in the $z = 1/4$ plane due to electrostatic repulsions. Finally, the $NbO_6$ octahedra are somewhat distorted (see bond lengths and bond angles in Table 4), but the average Nb–O distance, 1.973 Å, is typical of Nb (V) oxides. The unit cell dimensions of $a \approx b \approx 2a_p$ result from the tilting of

Table 4
Bond lengths and angles (refinement # 2)

| Bonds lengths (Å) | | Bond angles (°) | |
|---|---|---|---|
| Nb–$O_1$ | 2.061 | $O_1$–Nb–$O_2$ | 179.8 |
| Nb–$O_2$ | 1.892 | $O_3$–Nb–$O_4$ | 167.7 |
| Nb–$O_3$ | 2.006 | Nb–$O_5$–Nb | 165.6 |
| Nb–$O_4$ | 1.941 | Nb–$O_2$–Nb | 165.1 |
| Nb–$O_5$ | 1.969 | | |
| Mean Nb–O | 1.972 | | |

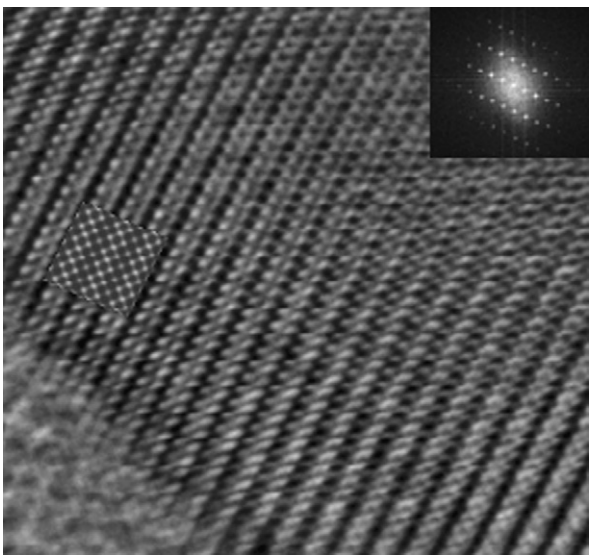

Fig. 7. Experimental image of $Nd_{1/3}NbO_3$ along the [100] projection. Inset in the image: simulated image obtained using the structural data determined by X-ray diffraction. Inset in the top-right angle shows the Fourier transform of the experimental image.

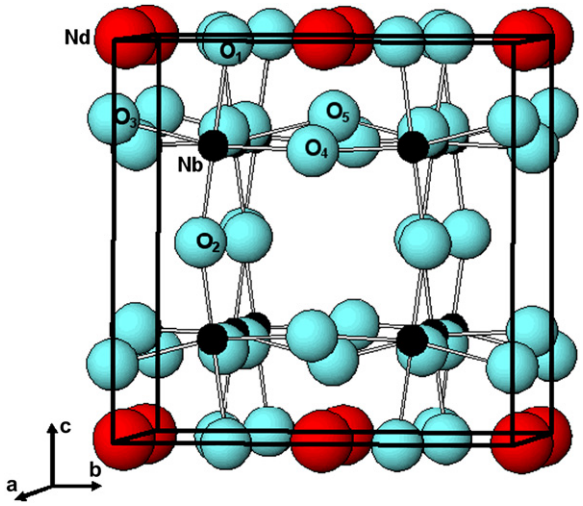


Fig. 8. Atomic arrangement in $Nd_{1/3}NbO_3$.

$NbO_6$ octahedra around the *b*-axis. The superlattice reflections arising from this small rotation are very weak in the X-ray diffraction pattern, due to the much stronger scattering factors of Nb and Nd.

The very weak and more or less diffuse scattering observed in the electron diffraction patterns probably indicates some long-range ordering of neodymium atoms and vacancies. Such additional reflections have already been observed by Alario-Franco et al. [10] for the A-deficient perovskite $Th_{1/4}NbO_3$. These authors interpreted their observation by considering a modulation of the occupation of the Th crystallographic sites associated with a displacive modulation of these atoms and also of surrounding atoms. Preliminary observations indicate that the additional reflections observed in $Nd_{1/3}NbO_3$ by electron diffraction are not located at the same position as those observed for $Th_{1/4}NbO_3$, which likely results from different stoichiometry of the compounds, i.e. the cationic occupation in the central site is different and thus the modulation should be different. One should also note that, due to the weakness of these additional diffuse reflections appearing in the electron diffraction patterns, their presence in X-ray diffraction patterns is doubtful. A single crystal study should now be performed to provide a more complete description of the structure.

## Acknowledgements

The ‘‘region Aquitaine’’ is acknowledged for its financial support. In addition, we are indebted to Éric Labraud for his technical assistance.

## References

[1] Roger H. Mitchell, Perovskites: Modern and Ancient, Almaz Press, Thunder Bay (Ontario, Canada), 2002.
[2] H. Yoshioka, J. Am. Ceram. Soc. 85 (2002) 1339.
[3] P.D. Battle, J.E. Bennett, J. Sloan, R.J.D. Tilley, J.F. Vente, J. Solid State Chem. 149 (2000) 360.
[4] B.J. Kennedy, C.J. Howard, Y. Kubota, K. Kato, J. Solid State Chem. 177 (2004) 4552.
[5] A.M. Abakumov, R.V. Shpanchenko, Mater. Res. Bull. 30 (1994) 97.
[6] C.C. Torardi, L.H. Brixner, C.M. Foris, J. Solid State Chem. 58 (1985) 204.
[7] E. Orgaz, A. Huanosta, J. Solid State Chem. 97 (1992) 65.
[8] A. Huanosta, E. Orgaz, Solid State Ionics 62 (1993) 69.
[9] P.N. Iyer, A.J. Smith, Acta Crystallogr. 23 (1967) 740.
[10] M.A. Alario-Franco, I.E. Grey, J.C. Joubert, H. Vincent, M. Labeau, Acta Crystallogr. A38 (1982) 177.
[11] M. Nakayama, Y. Uchimoto, M. Wakihara, J. Power Sources 146 (2005) 674.
[12] S. Garcia-Martin, F. Garcia-Alvarado, A.D. Robertson, A.R. West, M.A. Alario-Franco, J. Solid State Chem. 128 (1999) 97.
[13] S. Garcia-Martin, J.M. Rojo, H. Tsukamoto, E. Morán, M.A. Alario-Franco, Solid State Ionics 116 (1999) 11.
[14] A. Nadiri, G. Le Flem, C. Delmas, J. Solid State Chem. 73 (1988) 338.
[15] L. Carrillo, M.E. Villafuerte-castrejón, G. González, L.E. Sansores, J. Mater. Sci. 35 (2000) 3047.
[16] Z. Zhang, C.J. Howard, B.J. Kennedy, K.S. Knight, Q. Zhou, J. Solid State Chem. 180 (2007) 1846.